ElecSus: A program to calculate the electric susceptibility of an atomic ensemble

Mark A Zentile[a,*], James Keaveney[a], Lee Weller[a,b], Daniel Whiting[a], Charles S Adams[a], Ifan G Hughes[a]

[a]*Joint Quantum Center (JQC) Durham-Newcastle, Department of Physics, Durham University, South Road, Durham, DH1 3LE, United Kingdom*
[b]*Present address: Cavendish Laboratory, Department of Physics, University of Cambridge, J. J. Thomson Avenue, Cambridge CB3 0HE, United Kingdom*

Abstract

Presented is a computer program and underlying model to calculate the electric susceptibility of an alkali-metal vapour, which is essential to predict its absorptive and dispersive properties. We use a matrix representation of the atomic Hamiltonian in the completely uncoupled basis in order to calculate transition frequencies and strengths. The program calculates various spectra for a weak-probe laser beam in an atomic medium with an applied axial magnetic field. This allows many optical devices to be designed, such as Faraday rotators/filters, optical isolators and circular polarisation filters. Fitting routines are also provided with the program which allows the user to perform optical metrology by fitting to experimental data.

Keywords: Spectroscopy, Faraday effect, Atom-light interaction, Alkali atom, FADOF

PROGRAM SUMMARY

Program Title: ElecSus
Licensing provisions: Apache License, Version 2.0
Programming language: Python
Computer: Any single computer running Python 2.
Operating system: Linux, Mac OSX, Windows.
RAM: Depends on the precision required and size of the data set, but typically not larger than 50 MiB.
Number of processors used: from 1 to all available.
Keywords: Spectroscopy, Faraday effect, Atom-light interaction
Classification: 2.2, 2.3
External routines/libraries: SciPy library [1] 0.12.0 or later, NumPy [1], matplotlib [2]
Nature of problem:
Calculating the weak-probe electric susceptibility of an alkali-metal vapour. The electric susceptibility can be used to calculate spectra such as transmission and other Stokes parameters. Measurements of experimental parameters can be made by fitting to the theory.
Solution method:
The transition frequencies and wavelengths are calculated using a matrix representation of the Hamiltonian in the completely uncoupled basis. A suite of fitting methods are provided in order to allow user supplied experimental data to be fit to the theory, thereby allowing experimental parameters to be extracted.
Restrictions:
Only describes a magnetic field parallel to the laser beam propagation direction. Results are only valid in the weak-probe regime.
Running time:
At standard precision less than a second for just a theory plot, fitting will take 10 seconds to 20 minutes depending of the method used and the number of parameters to fit.

[1] T. E. Oliphant, Comput. Sci. Eng. 9, 10 (2007). http://www.scipy.org/
[2] J. D. Hunter, Comput. Sci. Eng. 9, 10 (2007). http://matplotlib.org/

*Corresponding author.
E-mail address:* m.a.zentile@durham.ac.uk

1. Introduction

Atomic physics of thermal vapours is an expanding field of interest, ranging from the fundamental to the applied. Examples of fundamental physics include observations of the co-operative Lamb shift [1], hyperfine Paschen-Back regime [2], macroscopic entanglement [3], collisional laser cooling [4] and dipole-dipole induced bistability [5] to name a few. Applications include compact and precise magnetometers [6] and clocks [7], laser frequency stabilisation both on [8] and off-resonance [9, 10], enhanced frequency up-conversion [11], trans-spectral orbital angular momentum transfer [12] and quantum memories [13, 14].

Most applications benefit from being able to predict the absorptive and dispersive properties (in absolute measures) of the medium. The electric susceptibility is key in calculating these properties [15]; here we present a fast and easy to use computer program, based on our model for the susceptibility of an atomic ensemble, that can be used to predict absorption and dispersion given certain parameters. This facilitates designing optical devices, such as Faraday filters [16–19] and optical isolators [20], without resorting to impractical trial and error. Also, since each theory curve will typically take less than a second to compute, fitting experiment to theory becomes practical. This allows experimental parameters to be measured efficiently. This has applications for optical magnetometry [21], optical thermometry [22–24], number density measurements in optically thick vapour [25, 26], and diagnostics for devices such as vacuum dispensers [27–29] and vapour cells [30–33].

In our group we have built up a theoretical model of the electric susceptibility [15] of an alkali-metal vapour that includes dipole-dipole induced linewidth broadening [34] and axial magnetic fields [35]. The model has been shown to be accurate at the ∼ 0.5% rms level when calculating the frequency dependence of transmission [15, 34] and Faraday rotation [10, 20, 35] for applied magnetic fields of up to ∼ 6000 G, and is not

expected to break down until the diamagnetic effect [36] becomes important ($> 10^7$ G). Fitting to the model has found utility in measuring number density [37] and large magnetic fields with high precision [10], and estimating buffer gas pressures in vapour cells [38]. Being able to extract shifts of many atomic transitions that overlap due to Doppler and self broadening was also key in observing the cooperative Lamb shift [1].

2. Theoretical background

The complex index of refraction, $n_c \equiv n + \mathrm{i}\beta$, of an optical medium is related to its electric susceptibility, χ, by the equation [39]

$$n_c = \sqrt{1 + \chi}. \qquad (1)$$

The real part (commonly known as the refractive index), n, gives the ratio of the speed of light in vacuum, c, to the phase velocity in the medium. The attenuation coefficient, α, is obtained from the imaginary part, β, by $\alpha = 2k\beta$ [39], where k is the angular wavenumber. The electric susceptibility of a medium is a function of frequency and hence gives rise to dispersion, as well as frequency dependent attenuation.

Another quantity of interest is the group index, n_g, which is defined as c divided by the group velocity. Calculating the group index allows one to estimate the speed of an optical pulse in the medium, and therefore is a useful quantity for slow light [40] or fast-light [41, 42] experiments. We can calculate n_g if we know n as a function of angular frequency ω by using the relation [43],

$$n_\mathrm{g} = n + \omega \frac{\partial n}{\partial \omega}. \qquad (2)$$

The spectral dependence of the electric susceptibility is therefore important to calculate. Both the real and imaginary parts have characteristic line-shapes which we will look at in the next section.

2.1. The Electric susceptibility line-shape

For a single transition of a stationary atom the imaginary part of the electric susceptibility, χ_im, has a line-shape profile given by a Lorentzian distribution [44] with a full width half maximum (FWHM), Γ. This width has contributions from natural broadening (Γ_0), dipole-dipole induced self broadening (Γ_self) [34] and any extra homogeneous broadening (Γ_ex) e.g pressure broadening due to buffer gasses. The real part of the susceptibility, χ_re, is characterised by a dispersive lineshape. The centre of these distributions occur at the resonance frequency of the transition (ω_i). However, the Doppler effect causes a moving atom to observe a shifted frequency. A thermal ensemble of atoms has a Gaussian distribution of velocities in the light propagation direction [45], therefore the resulting lineshape is obtained by a convolution of the Lorentzian and Gaussian profiles. This spectral lineshape of χ_im is known as a Voigt profile. It is important for the atom-light interaction to be in the weak-probe regime[1] or deviations from a Voigt profile

---

[1] To achieve the weak-probe regime it is not sufficient for the intensity to be lower than the saturation intensity [46], hyperfine pumping must also be absent [47, 48]

will be seen [49, 50]. Further deviations can also occur for large amounts of buffer gasses or short length cells due to Dicke narrowing [51]. These effects are beyond the scope of this work.

In room temperature ensembles of alkali atoms, the Gaussian broadening is roughly two orders of magnitude larger than the Lorentzian broadening. This would naively lead one to conclude that these spectra are insensitive to the Lorentzian component, but this is incorrect [34, 50]. Far from resonance the Lorentzian contribution to the Voigt profile dominates [52]. Insets i) and ii) of Figure 1 show the rubidium D_1 lineshape with and without Doppler broadening respectively.

For a more comprehensive guide on how to construct the electric susceptibility for a single transition see ref. [53]. Here we quote the result that for transition i, the susceptibility is proportional to a relative transition strength factor, c_i^2, multiplied by the Faddeeva function, $w(z)$, like so

$$\chi_i(\Delta_i) = \mathrm{i} c_i^2 \frac{d^2 \mathcal{N}_a}{\hbar \epsilon_0} \frac{\sqrt{\pi}}{kU} w(\zeta), \qquad (3)$$

$$\zeta = \frac{\mathrm{i}}{2} \frac{\Gamma}{kU} + \frac{\Delta_i}{kU}, \qquad (4)$$

where d is the reduced dipole matrix element [15], $\mathcal{N}_a$ is the number density of identical atoms, $\hbar$ is the reduced Planck's constant, ϵ_0 is the vacuum permittivity, Δ_i is the angular detuning from resonance, defined as $\Delta_i \equiv \omega - \omega_i$ where ω is the angular frequency of the light and ω_i is the resonance angular frequency of transition i. U is the $1/e$ width of the Gaussian velocity distribution, given by $U = \sqrt{2k_\mathrm{B}T/m}$, where k_B is Boltzmann's constant, T is the thermodynamic temperature and m is the mass of the atom. Note that $\mathcal{N}_a$ can be calculated from the elemental number density $\mathcal{N}$ (see Appendix A) by the following equation,

$$\mathcal{N}_a = \frac{F_a \mathcal{N}}{2(2I + 1)}, \qquad (5)$$

where F is the isotopic fraction and I the nuclear spin quantum number. The denominator, $2(2I + 1)$, is the number of states in the ground manifold since we expect the atoms to be distributed evenly among all the these states. This is justified by calculating the Boltzmann factor. For easily accessible magnetic fields and temperatures for thermal vapours, this factor deviates from 1 at the 0.1% level for states in the ground manifold and at the 10^{-13} level for states between the ground and excited manifolds. Note that when not in the weak-probe regime, hyperfine pumping will occur and redistribute populations.

To calculate the total susceptibility we add the contribution from all transitions ($\chi = \sum_i \chi_i$). We then write the susceptibility in terms of a global detuning, Δ, which is the frequency relative to a defined global linecentre. For convenience we have chosen zero detuning to occur at the weighted linecentre for D_1 ($n^2S_{1/2} \rightarrow n^2P_{1/2}$) and D_2 ($n^2S_{1/2} \rightarrow n^2P_{3/2}$) transitions (see Appendix B) where n = 3, 4, 5 or 6 for sodium, potassium, rubidium or caesium respectively. We now look at using the atomic Hamiltonian to calculate the frequencies of the transitions relative to the linecentre as well as their strengths.

2.2. The atomic Hamiltonian

The atomic Hamiltonian is written as a sum of all interaction mechanisms,

$$H = H_0 + H_{\mathrm{f}} + H_{\mathrm{hf}} + H_{\mathrm{Z}}, \qquad (6)$$

where H_0 is the coarse atomic energy and H_{f}, H_{hf} and H_{Z} are the fine, hyperfine and external magnetic field interactions respectively. The fine structure interaction can be written as

$$H_{\mathrm{f}} = \frac{\gamma_{\mathrm{f}}}{\hbar^2} \left(\boldsymbol{L} \cdot \boldsymbol{S} \right), \qquad (7)$$

where $\boldsymbol{L}$ and $\boldsymbol{S}$ are the orbital and spin angular momenta of the valence electron respectively, γ_{f} is the spin-orbit constant for the particular atom. The hyperfine interaction has contributions from the magnetic dipole interaction, H_{d}, and electric quadrupole interaction, H_{q}, ($H_{\mathrm{hf}} = H_{\mathrm{d}} + H_{\mathrm{q}}$). We have omitted higher order multi-pole interactions since their effect is small ($\Delta E / \hbar < 1$ kHz [54]). The magnetic dipole interaction can be written as [36]

$$H_{\mathrm{d}} = \frac{A_{\mathrm{hf}}}{\hbar^2} \left(\boldsymbol{I} \cdot \boldsymbol{J} \right), \qquad (8)$$

where A_{hf} is the magnetic dipole constant, and $\boldsymbol{I}$ and $\boldsymbol{J}$ are the nuclear spin and total electron ($\boldsymbol{J} = \boldsymbol{L} + \boldsymbol{S}$) angular momenta respectively. Using the convention that the magnitude of an arbitrary angular momentum $\boldsymbol{K}$ is $\sqrt{K(K+1)}\hbar$, the electric quadrupole interaction can be written as [36]

$$H_{\mathrm{q}} = \frac{B_{\mathrm{hf}}}{\hbar^4} \left[\frac{3(\boldsymbol{I} \cdot \boldsymbol{J})^2 + \frac{3}{2}(\boldsymbol{I} \cdot \boldsymbol{J})\hbar^2 - I(I+1)J(J+1)\hbar^4}{2I(2I-1)J(2J-1)} \right], \quad (9)$$

where B_{hf} is the electric quadrupole constant. See Appendix B for values for A_{hf} and B_{hf}. The interaction with an external magnetic field is given as

$$H_{\mathrm{Z}} = \frac{\mu_{\mathrm{B}}}{\hbar} \left(g_L \boldsymbol{L} + g_S \boldsymbol{S} + g_I' \boldsymbol{I} \right) \cdot \boldsymbol{B}, \qquad (10)$$

where μ_{B} is the Bohr magneton, and g_L, g_S and g_I' are the g-factors corresponding to the electron orbital, electron spin and nuclear angular magnetic moments. g_L is taken to be 1; the values for the other g-factors are given in Appendix B. If we choose our quantization axis to be parallel to the magnetic field, equation 10 reduces to

$$H_{\mathrm{Z}} = \frac{\mu_{\mathrm{B}}}{\hbar} \left(g_L L_z + g_S S_z + g_I' I_z \right) B_z. \qquad (11)$$

Once the Hamiltonian is constructed, we need to find the eigenvalues, E_j, and corresponding eigenstates, $|j\rangle$, in order to calculate the transition energies and strengths. The transition energy is simply the difference is energy between the ground and excited states ($E_{\mathrm{e}} - E_{\mathrm{g}}$).

2.2.1. Calculating transition strengths from the eigenstates

The eigenstates will be given by some combination of completely uncoupled basis states $|L, m_L, m_s, m_I\rangle$, where m_L, m_S and m_I are the z-projection quantum numbers. Transition strengths are given by the electric dipole matrix element squared, $\left| \langle \mathrm{g} | er_q | \mathrm{e} \rangle \right|^2$, where er_q is the component of the dipole

operator in the spherical basis (see equation 5.17 in [44]); this chooses whether the transition is σ^+, σ^- or π ($\Delta m_L = -q$ where $q = -1, +1$ or 0 respectively). To illustrate how the strength is calculated, we take the example of a σ^- transition between the eigenstates

$$|g\rangle = a_1 |0, 0, +\tfrac{1}{2}, -\tfrac{1}{2}\rangle + a_2 |0, 0, -\tfrac{1}{2}, +\tfrac{1}{2}\rangle \qquad (12)$$

$$|e\rangle = b_1 |1, -1, +\tfrac{1}{2}, -\tfrac{1}{2}\rangle + b_2 |1, +1, -\tfrac{1}{2}, -\tfrac{3}{2}\rangle$$
$$+ b_3 |1, 0, -\tfrac{1}{2}, -\tfrac{1}{2}\rangle + b_4 |1, 0, +\tfrac{1}{2}, -\tfrac{3}{2}\rangle \qquad (13)$$

where a_1, a_2, b_1, b_2, b_3 and b_4 are parameters which are known after finding the eigenvalues and eigenstates of the Hamiltonian. Note that this choice of eigenstates is analogous to the $|1, 0\rangle \rightarrow |1, -1\rangle$, D_1 transition, in the $|F, m_F\rangle$ coupled basis in rubidium-87. The transition strength will be given by

$$\left| \langle g | er_1 | e \rangle \right|^2 = a_1^2 b_1^2 \left| \langle 0, 0, +\tfrac{1}{2}, -\tfrac{1}{2} | er_1 | 1, -1, +\tfrac{1}{2}, -\tfrac{1}{2}\rangle \right|^2. \qquad (14)$$

All other terms are zero since the er_1 operator can only couple states where the excited m_L quantum number is reduced by one and all other quantum numbers are the same. Since only the orbital angular momentum of the electron is changed during an electric dipole transition, we can decouple the transition into angular and spin parts,

$$\left| \langle g | er_q | e \rangle \right|^2 = a_1^2 b_1^2 \left| \langle L, m_L | er_q | L', m_L' \rangle \langle m_S, m_I | m_S', m_I' \rangle \right|^2, \qquad (15)$$

where symbols with a prime denote the excited state quantum number. The last part in equation (15) ensures that the only non-zero result comes when the electron spin and nuclear spin remain unchanged. Using the Wigner-Eckart theorem [44] we can reduce the angular part,

$$\left| \langle L, m_L | er_q | L', m_L' \rangle \right|^2 = \begin{pmatrix} L & 1 & L' \\ -m_L & q & m_L' \end{pmatrix}^2 \langle L \| er \| L' \rangle^2. \quad (16)$$

The symbol in brackets is a Wigner 3-j symbol [55]. When $L' = 1$ and $L = 0$, the square of the Wigner 3-j symbol is $1/3$ for any σ^+, σ^- or π transition. The double-bar matrix element, $\langle L \| er \| L' \rangle$, denotes the reduced dipole matrix element, d. Therefore, for our particular example the transition strength is simply,

$$| \langle g | er_1 | e \rangle |^2 = \frac{1}{3} d^2 a_1^2 b_1^2 \equiv d^2 c_i^2. \qquad (17)$$

Recalling equation (3), we see how the strength fits in to the amplitude of the electric susceptibility for a single transition. For the general case we find the strength from $d^2/3$ multiplied by $\sum_{i,j} a_i^2 b_j^2$, where a_i and b_j are the coefficients of two basis states which are allowed by the selection rules.

See section 3.2 for details of how ElecSus calculates this strength factor using a matrix representation of the Hamiltonian. Note that our program considers the case where the magnetic field is parallel to the propagation axis of the light, which means that π transitions are forbidden [36].

Figure 1 shows an example for the rubidium D_1 line, showing the result of of adding the lineshape at each transition frequency, scaled by the relative transition strength.
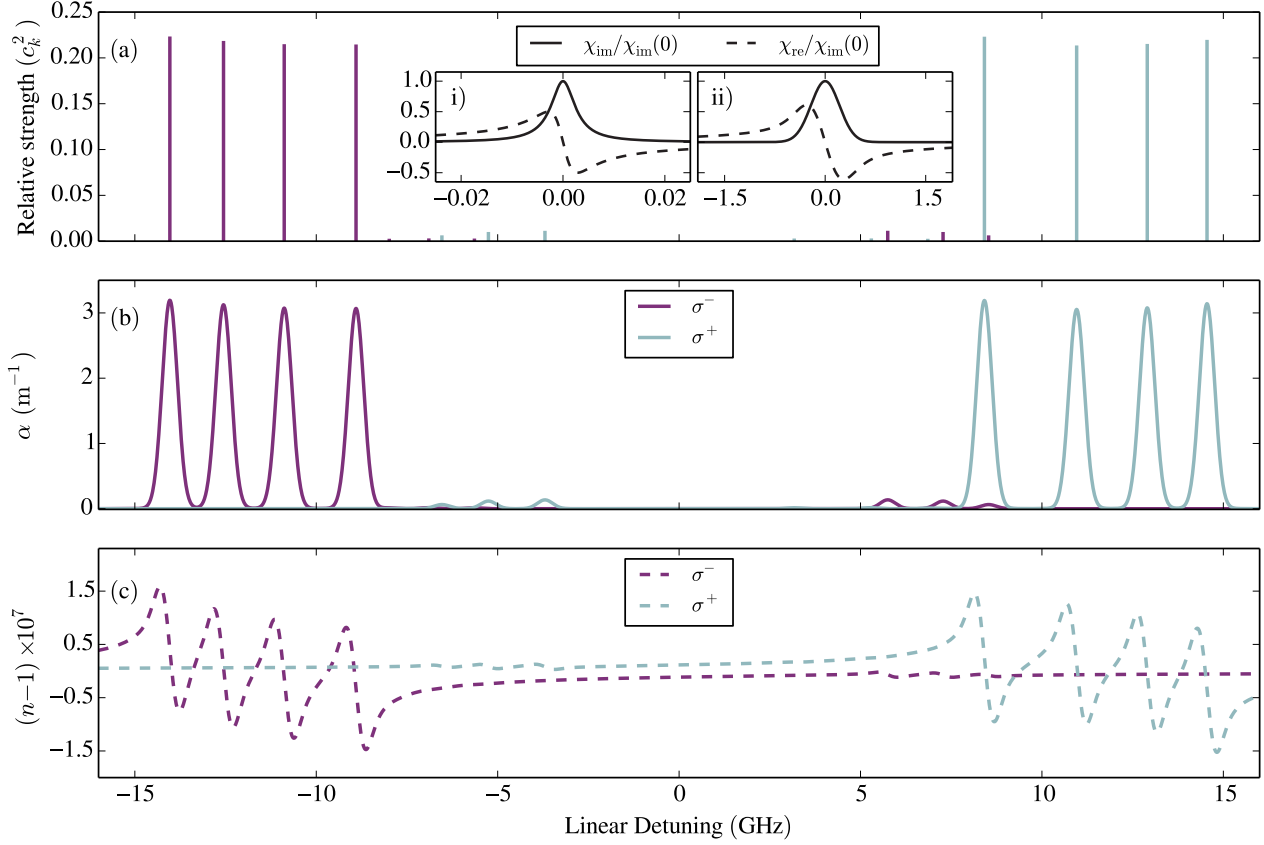
Figure 1: (Colour online) Graphs showing how the refractive indices and absorption coefficients are found as a function of global detuning ($\Delta/2\pi$). Panel (a) is a stick spectrum showing the transition frequencies which are calculated from finding the eigenenergies of the Hamiltonian of ^{87}Rb in a 6000 G magnetic field. The transition strengths are also found from the Hamiltonian (described in section 2.2). Inset i) of panel (a) shows the Doppler-free complex lineshape profile for ^{87}Rb on the D$_1$ line. Doppler broadening is added by convolving the lineshapes in i) with a Gaussian resulting in the lineshapes given in ii), (both insets are normalised to the peak of their respective imaginary part). The lineshapes in ii) are then simply added to the spectrum at the position of the transitions multiplied by their strength. This yields the extinction coefficient shown in panel (b) or the refractive index shown in panel (c).

2.3. The Stokes parameters

$$S_0 \equiv (I_- + I_+)/I_0, \tag{18a}$$

$$= \left(I_x + I_y\right)/I_0, \tag{18b}$$

$$= (I_\nearrow + I_\searrow)/I_0, \tag{18c}$$

$$S_1 \equiv \left(I_x - I_y\right)/I_0, \tag{18d}$$

$$S_2 \equiv (I_\nearrow - I_\searrow)/I_0, \tag{18e}$$

$$S_3 \equiv (I^- - I^+)/I_0, \tag{18f}$$

Together, the four Stokes parameters characterise the polarization state of light [56]. They are easily measurable with linear optics and photodetectors [57], and are therefore a convenient way to measure the polarization of light. However, the Stokes parameters have uses beyond measuring polarization. Predicting their spectral dependence for an atomic medium is useful since they can be used for several optical devices. The S_0 parameter, equivalent to transmission, can be used for primary thermometry [22]. The S_1 and S_2 parameter signals can be used as far off-resonance laser frequency stabilising references [9], while the S_3 signal is the dichroic atomic vapour laser lock [58, 59] error signal. The Stokes parameters are defined as

where the I_x and I_y are the intensities of light that are transmitted and reflected, respectively, at a polarising beam-splitter placed after the medium; this defines the x- and y-axes. $I_\nearrow$ and $I_\searrow$ are the intensities of light after the medium which are polarised at an angle that deviates from the x-axis by 45° and −45° respectively. I_- and I_+ represent the intensities of light which drive $\sigma^\pm$ transitions. I_0 is the intensity of light before entering the medium. Since ElecSus only considers $\sigma^\pm$ transitions, the medium is circularly birefringent and dichroic. It is therefore convenient to parametrise the initial polarisation of the light in terms of the two circular components,

$$\boldsymbol{E}_0 = E_- \mathbf{e}_- + E_+ \exp\left(i\phi_0\right)\mathbf{e}_+, \tag{19}$$

4

where E_0 is the electric field before the atomic medium and is written as a Jones vector [60, 61] in the the circular basis, and ϕ_0 is the phase shift between the two circular components. It is useful to define a quantity (p) representing the proportion of light that drives σ^- transitions,

$$p \equiv \frac{|E_-|^2}{|E_-|^2 + |E_+|^2}. \tag{20}$$

We can now write the Stokes parameters in terms of p and the extinction coefficients, $\alpha^\pm$, and refractive indices $n^\pm$,

$$S_0 = p \exp\left(-\alpha_- \ell\right) + (1-p) \exp\left(-\alpha_+ \ell\right), \tag{21a}$$

$$S_1 = 2\sqrt{p - p^2} \cos\left(2\psi\right) \exp\left[-\frac{1}{2}\left(\alpha_- + \alpha_+\right)\ell\right], \tag{21b}$$

$$S_2 = 2\sqrt{p - p^2} \sin\left(2\psi\right) \exp\left[-\frac{1}{2}\left(\alpha_- + \alpha_+\right)\ell\right], \tag{21c}$$

$$S_3 = p \exp\left(-\alpha_- \ell\right) - (1-p) \exp\left(-\alpha_+ \ell\right), \tag{21d}$$

$$\psi = \frac{1}{2}(n_+ - n_-)k\ell + \theta_0, \tag{21e}$$

where ℓ is the length of the medium in the propagation direction and $\theta_0 = \phi_0/2$. For linearly polarised light incident on the medium, θ_0 represents the angle the plane of polarization makes with the x-axis. We can then calculate the individual I_x and I_y spectra using the definitions (18b) and (18d),

$$I_x = (S_0 + S_1)/2 \tag{22}$$

$$I_y = (S_0 - S_1)/2. \tag{23}$$

These spectra are useful since they correspond to Faraday filtering [16–19].

3. Program structure

The program is centred on the `elecsus.py` module. This module takes the user-specified parameters and settings from the run card, imports the `spectrum` function and uses it to generate the spectrum, or imports the fitting modules which fit user data to curves generated by `spectrum`. Experimental data supplied by the user should be as a two-column comma separated values (csv) file; the first column specifies linear detuning in units of GHz while the second is the corresponding value for the spectrum. csv files are readable by spreadsheet programs and are a common data output format on digital storage oscilloscopes. The program then creates a new sub-directory for the output files. It writes the main result to a csv file named by the user-specified label suffixed by _theory.csv. If requested in the run card, the module also uses `matplotlib` [62] to plot the curve and display it to the screen; there is also an option to save the plot to a file. If a fit was performed the module will also save the residuals [63] of data and theory curves as a csv file, as well as output the fit parameters to a file suffixed by _Parameters.txt. Figure 2 shows a flowchart of the program structure.
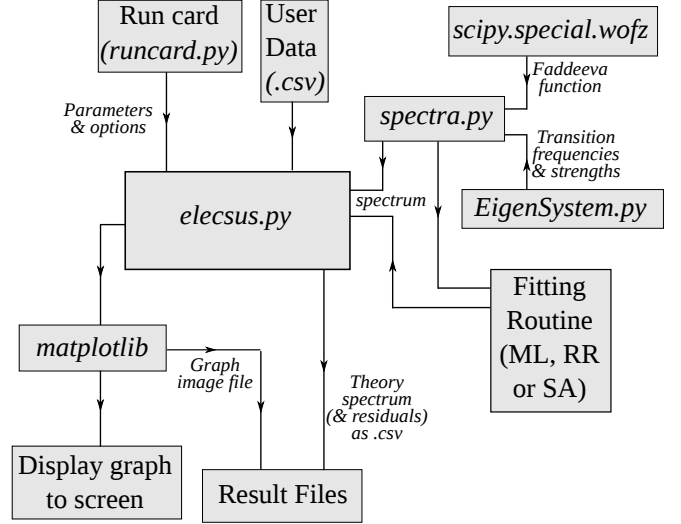

Figure 2: Block diagram showing the flow of information in the ElecSus program.

3.1. Global lineshape profile

In section 2.1 we saw that calculating the atomic lineshapes relies on calculating the Faddeeva function. Calculating the global lineshape must be done with care since an inefficient implementation can be slow. ElecSus does this by calling the `scipy.special.wofz` function, which is a wrapper for a fast algorithm written in C++ [64]. The lineshape should be the same for all transitions of the same atom and so the `wofz` function only needs to be called once per isotope. Isotopes of the same element will also have a slightly different lineshape because the different masses provide a different Doppler broadening. The appropriate lineshape profile is then added to the spectrum for each transition with a shift given by the transition detuning and an amplitude proportional to it's line-strength.

3.2. Matrix representation of the atomic Hamiltonian

For each atomic term ($n^2S_{1/2}$ and n^2P) a separate Hamiltonian is built up in a similar manner as described in section 2.2 as a matrix in the completely uncoupled basis. Each matrix is of size $D_{LSI} \times D_{LSI}$ where $D_{LSI} = (2L+1)(2S+1)(2I+1)$. We set the coarse atomic energy to zero since we are simply looking for the detuning values from a global linecentre. For the $n^2S_{1/2}$ term $L = 0$, so there is no fine structure interaction. The Hamiltonian is therefore given by

$$\hat{H}_S = \frac{A_{hf}}{\hbar^2}\left(\boldsymbol{I} \cdot \boldsymbol{J}\right) + \frac{\mu_B B_z}{\hbar}\left(g_S \hat{S}_z + g'_I \hat{I}_z\right). \tag{24}$$

ElecSus calculates D_1 and D_2 spectra separately, however the full n^2P term is calculated. The eigenvalues of the fine structure part of the Hamiltonian are $-\gamma_f$ and $\gamma_f/2$, but since we want to calculate detuning values from a global linecentre we need to cancel this energy. When addressing the $n^2P_{1/2}$ term we therefore calculate the Hamiltonian as

$$\hat{H}_P = \frac{\gamma_f}{\hbar^2}\left(\boldsymbol{L} \cdot \boldsymbol{S}\right) + \hat{H}_{hf} + \hat{H}_Z + \gamma_f \otimes \mathbb{I}_{D_{LSI}}, \tag{25}$$

5

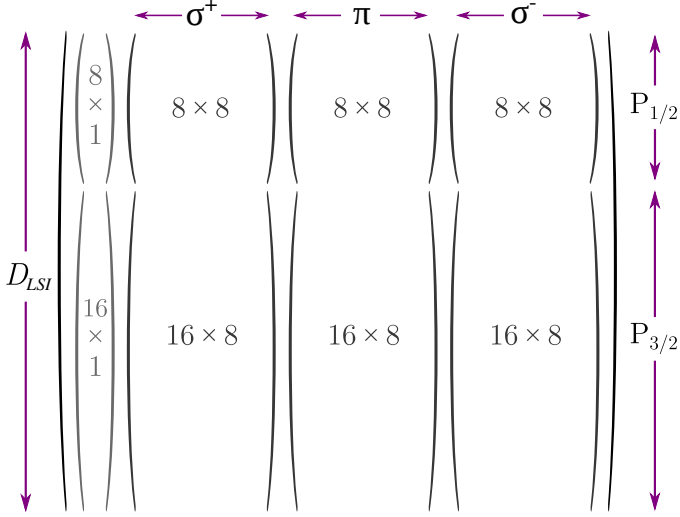Figure 3: A schematic of the n²P term matrix for ⁸⁷Rb obtained once diagonalised. The first column gives the eigenenergies which are added to the left of the matrix. The corresponding rows give the coefficients of the (completely uncoupled) basis states that make up the eigenstate. Certain parts of the matrix correspond to allowed final states for transitions, and so are post selected when finding transition strengths. In this case the sub-matrices are 8 by 8 for a D_1 transition and 16 by 8 for D_2.

Figure 4: (Colour online) The extinction coefficient as a function of linear detuning ($\Delta/2\pi$) for a ⁸⁷Rb vapour on the D_1 line and at a temperature of 20 °C. There are seven plots of the extinction coefficient at magnetic field values ranging from 0 to 0.3 T in increments of 0.05 T. Note that 1 T = 10^4 G. Each plot is placed on its side, displaced to the right for clarity, with the extinction coefficient ranging from 0 to 5 m⁻¹ in each one. The area under each curve has been coloured either translucent red or blue, representing σ^- and σ^+ transitions. Overlaying the plots are curves showing the transition frequencies as a function of magnetic field. Notice that the strong σ^- transitions move to lower energies while the strong σ^+ ones move to higher energies. A video showing the evolution of the extinction coefficients for a Caesium vapour is available to download from http://www.jqc.org.uk/resource/elecsus/12683

where $\mathbb{I}_{D_{LSI}}$ is the identity matrix. If we instead wanted to address the n²P$_{3/2}$ term we would introduce a $-\gamma_f/2 \otimes \mathbb{I}_{D_{LSI}}$ term. Figure 3 shows a schematic of the $\hat{H}_P$ matrix after it is diagonalised. When calculating transition strengths, certain parts of the $\hat{H}_P$ matrix are selected depending on whether we want to calculate σ^+ or σ^- transitions, and which D-line. Each strength factor (c_i) is then calculated by performing the dot product between one of the rows of $\hat{H}_S$ with one of the post-selected rows of the excited state matrix. Many strength factors will be zero (with some numerical computing error) and as such a lower bound on the strength is placed in order to reject these transitions and save computing time. Also, the transition strengths corresponding to π transitions are not calculated since they are forbidden. It should be noted that in the case of a zero magnetic field ElecSus adds a very small magnetic field (10^{-4} G) in order to discriminate between the energy levels. This is necessary in order to perform the post-selection. It should also be highlighted that even though we calculate the full P-term Hamiltonian, we cannot use this to calculate both D_1 and D_2 spectra at the same time, as might be expected. This is because the hyperfine coefficients used for the n²P$_{1/2}$ term are different to those for the n²P$_{3/2}$ term. The omission of lithium spectra from the current version of ElecSus is partly due to this reason. ElecSus treats D_1 and D_2 spectra separately, but lithium D_1 and D_2 lines are sufficiently close (∼ 10 GHz) that they need to both be included when predicting a single spectrum.

To demonstrate the power of the Hamiltonian technique we show in figure 4 extinction coefficient calculated by ElecSus for increasing values of the magnetic field. At small and large magnetic field values the spectra are simple, and can be defined by good quantum numbers [38]. In these regimes, it may be sufficient to estimate frequency shifts by a perturbative treatment.
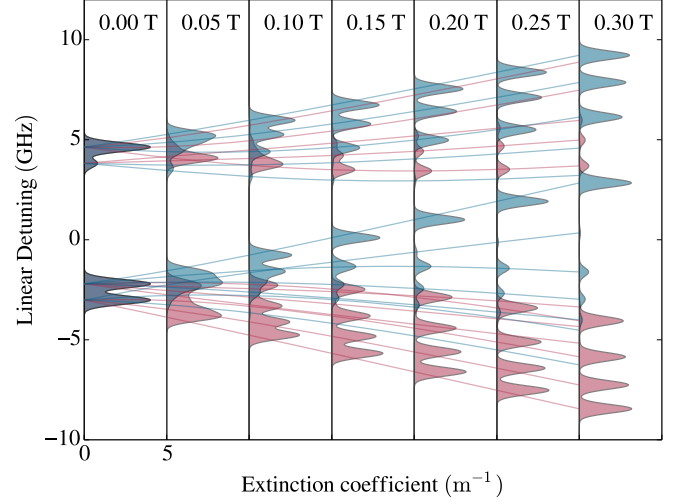
However, in the intermediate regime there are no good quantum numbers, and neither the hyperfine interaction nor the magnetic interaction can be considered small. This shows the power of the Hamiltonian technique in being able to find transition frequencies and strengths accurately in all regimes.

3.3. Fitting experimental spectra and timing information

The user provides experimental data, in csv format, as two columns of values. The first column specifies the linear detuning (in GHz) while the second gives the spectrum data. If a different linecentre value (from that specified in Appendix B) has been used to make the linear detuning axis, the user can specify a global shift in the run card in order to take this into account.

Fitting theory to experiment involves defining a 'cost' function, which quantifies how far the theory curve deviates from the experimental. This is often defined as the square of the difference between theory and experiment summed at each point along the curve. The cost function is then minimised by changing the parameters which define the theory curve. It is useful to think of this as finding the global minimum in a parameter space. There are three different fitting routines that can be used and should be selected based on the complexity of the fitting problem. A more complex fitting problem will tend to be one with many fit parameters.

In simple cases the option of fitting via the Marquardt-Levenberg (ML) method [63] should be chosen. This method is a 'hill-climbing' algorithm, which will quickly find the lo-
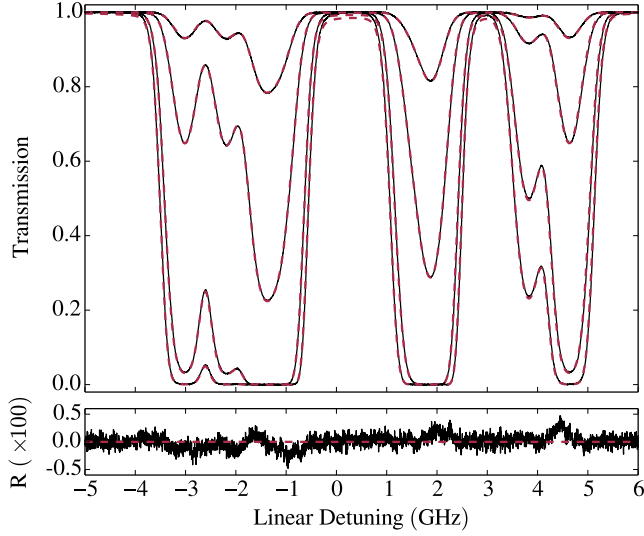
Figure 5: Plots of transmission versus detuning on the D_1 line for four different temperatures of a 75 mm long rubidium vapour cell with natural isotopic abundance. The (black) solid line shows experimental data while the (red) dashed curves are theoretical results using ElecSus with temperature as the only fit parameter. Lower curves correspond to higher temperatures; the temperatures were found to be 18.6 °C, 36.1 °C, 59.8 °C and 69.3 °C. Underneath the residuals (R between experiment and theory are plotted for the 18.6 °C data set (rms deviation of 0.1%).

Figure 6: (Colour online) Transmission as a function of linear detuning on the D_1 line for an isotopically enriched ^{87}Rb cell (1.0 % ^{87}Rb, 99.0 % ^{85}Rb) with an internal length of 1 mm. The solid (black) shows the experimental data while the dashed (blue) and dotted (purple) lines show fits to the theory using the RR and ML fitting routines. rms deviations from the experimental data of 0.5% and 1% were found for the RR and ML fits respectively. The fit parameters were the magnetic field, cell temperature, and extra Lorentzian broadening due to buffer gases.

cal minimum (or maximum, hence the name). Figure 5 shows four different experimental transmission spectra taken at different temperatures. These temperatures were then found by fitting using the ML method. Typically, when fitting one parameter we find no further improvement by using the global fitting routines. One exception to this is the case of fitting high magnetic fields, where the ML technique can fail unless the initial guess is accurate. This is because there may be little or no overlap between the experimental and initial theoretical prediction, creating a plateau in parameter space which is known to be hard for hill-climbing algorithms to deal with [65].

For more complicated fits of more parameters the ML technique may fail to find the global minimum, and so a global fitting routine should be used. Figure 6 shows the result of fitting three experimental parameters using the ML method and the random-restart [65] (RR) method. The random-restart method is a meta-algorithm which simply performs an ML fit for a range of randomly generated initial states, then picks the best fit. In this way the RR technique has the possibility of escaping the nearest minimum. Another advantage of this method is that it is easily parallelised and can therefore be more time efficient; ElecSus will use all available cores in the computer's processor in order to perform an RR fit.

Another global fitting routine supplied ElecSus is based on simulated annealing (SA) [66]. It uses the Metropolis algorithm [67] with a $T_{n+1} = T_n/(1 + \delta T_n)$ cooling schedule [68] where δ is simply a small number. Figure 7 shows an experimental S_1 spectrum fitted to theory with four fit parameters, using both the ML and SA techniques. The ML method clearl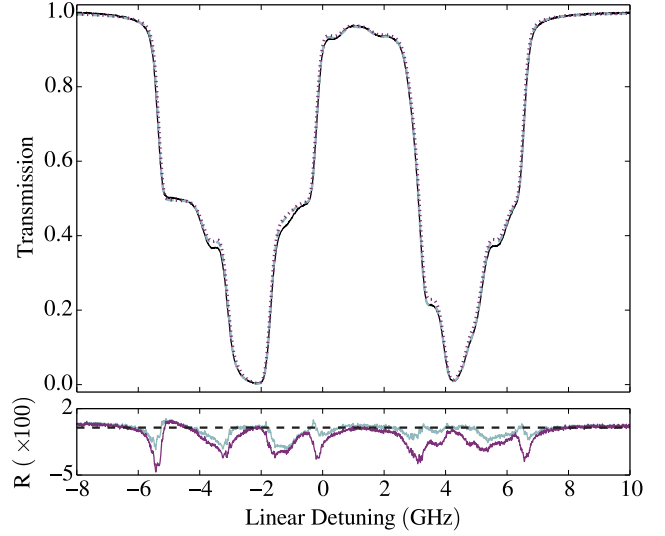y does not perform as well as the SA method. ElecSus' RR routine was found to be unreliable when applied to this particular data, but on occasion did manage to find a good fit.

To compare the speed of the different fitting routines the data provided in figure 6 was fit to theory using all three fitting routines, with the same precision (10 MHz) and the same number of points (4774). A computer with an Intel® Core™ i3-3220 processor was used. The time taken was found to be 13 seconds, 80 seconds and 10 minutes for the ML, RR and SA techniques respectively. Note that the RR technique involves evaluating spectra in parallel (4 parallel processes in this case) whilst the other two are sequential.

3.3.1. Uncertainties in fit parameters

When fitting experiment to theory a χ^2 analysis [63] is often used to extract the statistical uncertainty in the fit parameters. This requires knowledge of the uncertainty of the data points which will vary from experiment to experiment. The current version of ElecSus has no facility to accept these uncertainties as an input and so does not provide uncertainties in the fit parameters. However, since ElecSus outputs the theoretical curve as csv file, the user can perform this analysis manually (see ref. [63]).

Another method to extract the statistical uncertainty in the fit parameters is to take several data sets under the same experimental conditions and fit them independently. Then the mean and standard error of each parameter can be found.

4. Installation and usage

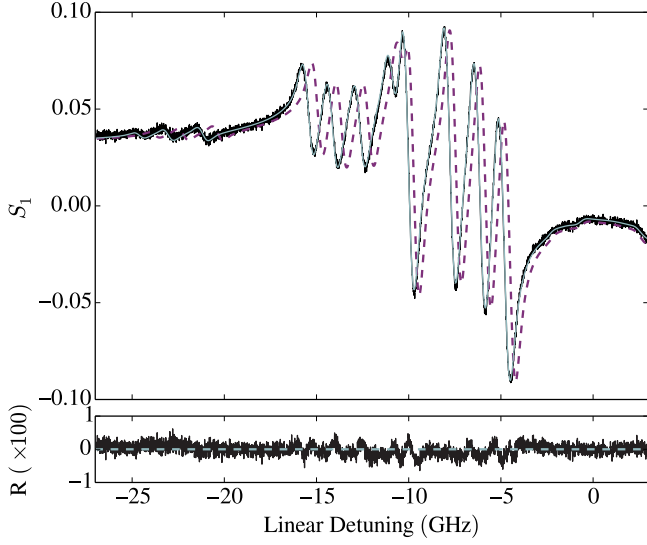The program can be downloaded from http://www.jqc. org.uk/resource/elecsus/12683 as a zip file named

Figure 7: (Colour online) S_1 stokes parameter as a function of linear detuning on the D_2 line for a ^{87}Rb cell (99.0 % ^{87}Rb, 1.0 % ^{85}Rb) with a length of 1 mm. The solid (black) line is the experimental data while the solid (blue) and dashed (purple) lines are the fits to theory using the SA and ML techniques respectively. The ML fit is clearly poor; shown underneath are the residuals for the SA fit. The rms deviations of the ML and SA fits were 2.2% and 0.16% respectively.

`ElecSus.zip`. Installation should be complete after simply extracting the `ElecSus.zip` file. No further action is required since it is assumed that the prerequisites (NumPy, SciPy and Matplotlib) are installed, and are found by the python interpreter. To use the program, the following steps should be taken.

1. Open a command prompt window and move to the directory extracted from the zip file (main directory).
2. Copy the file `runcard.py` to create your own file `myruncard.py`.
3. If fitting is required, place the csv file containing the data in the main directory.
4. Change the values and options in the file `myruncard.py` to the desired ones.
5. Execute the following command in the prompt window:

   ```
   python elecsus.py myruncard.py
   ```

   If the `myruncard.py` option is omitted the program will, by default, look in `runcard.py` for parameter values and options.

4.1. Run card parameters and options

In the run card the user must specify which alkali element, D-line and spectrum they want to compute. The choices of spectra for ElecSus to compute are the refractive indices, $n^{\pm}$, the group indices, $n_g^{\pm}$, Stokes parameters and the individual I_x and I_y spectra. The user can then specify parameters such as temperature, cell length etc. and whether they would like to fit to experimental data or simply produce a theoretical prediction. The variables in the run card are python variables, and as such the order in which they are specified does not matter.

We should note that there are two temperature variables, one which parametrises the number density (see Appendix A) and one which parametrises the Doppler broadening, where the second is constrained to the first by default. The option to treat these two temperatures separately is included for two reasons. The first reason is that non-uniform heating of vapour cells can cause the vapour temperature near the laser beam to be different to the temperature at or near the metal reservoir. The second reason is that the number density formulas used are only quoted to be accurate to about 5% [69], and so when fitting to a sufficiently accurate and precise experimental spectrum we would expect the two temperatures to disagree even if the whole cell is in thermal equilibrium. This disagreement would correspond to the systematic error in the vapour pressure formula.

It should also be noted that not all the options are relevant, and in these cases ElecSus will ignore those entries. For example when fitting to data the options that define the detuning axis are ignored since this is defined by the first column of the csv data file provided by the user. However, these variables should not be deleted from the run card.

4.2. Description of examples

Provided with ElecSus are two sets of experimental data taken using the same experimental procedure as described in reference [10]. Also provided are two sample run cards, which can immediately be used by the user to ensure the program is working on their computer.

The first example can be run by executing the following command in a prompt window whilst in the main directory:

```
python elecsus.py runcard_D1sample.py
```

This will use the data provided in the data file `SampleDataRbD1.csv`, and then fit three parameters using the RR method. Since this data is the same as shown in figure 6, and the same parameters are being fitted, the result should be very similar to that found in figure 6. Fitting should not take longer than a few minutes.

In a similar way the user can run the second example with the `runcard_D2sample.py` file. This will use data from the `SampleDataRbD2.csv` file, which is the same as the data shown in figure 7. Running this example will fit the data using the SA technique and should give a correspondingly similar result to that seen in the figure. Note that this example can take up to 30 minutes to run.

5. A further application: Pulse propagation

To highlight the power of ElecSus we follow an example where we have used it to design a laser frequency stabilising signal and also extract key information about the experimental cell in order to accurately predict weak-probe pulse propagation. To demonstrate this a 2 mm long rubidium vapour cell with natural isotopic abundance was heated, and then nanosecond long pulses (generated using a Pockels cell between two crossed polarisers) were sent through the medium. This experiment is very similar to that performed in ref. [42].

To find how a pulse propagates through the medium we must know how the transmission and refractive index of the medium vary across the bandwidth of the pulse. A Fourier transform of the temporal pulse profile gives the pulse profile in terms of frequency, and then the effect of transmission and phase shifts can be applied. An inverse Fourier transform then yields the pulse after traversing the medium.

To measure the required transmission and refractive index spectra, a weak continuous laser beam was sent through the medium and the transmission of the beam was measured as a function of laser frequency (see inset (a) of figure 8). ElecSus was then used to fit this spectrum to find the two temperatures that parametrise number density and the Doppler broadening. These were found to be 179.4 °C and 189.6 °C respectively, which indicates asymmetric heating of the cell. ElecSus can then be used again to infer what the refractive index of the medium should be given these parameters.

To measure the pulse profile accurately enough, single photon counting modules with good timing resolution were used. To build up an acceptable profile, counting was done over ∼ 15 minutes for approximately 100k repetitions. Over this length of time the laser frequency needs to be actively stabilised in order to prevent the carrier frequency of the pulse from drifting. We use a technique similar to that described in ref. [9]. The experimental parameters required to give suitable frequency references were found using ElecSus. We found that using the S_1 Stokes parameter with temperatures around ∼ 140 °C and magnetic fields around 200 G, gave zero crossings both far off resonance and near zero detuning when using a 75 mm long rubidium vapour cell. This is useful since the near zero detuning reference can be used to demonstrate slow-light while the far off resonance reference is a good approximation to the reference pulse (defined as a pulse that traversed vacuum instead of the atomic medium). Inset (b) of figure 8 shows the raw photodetector signal used as the the frequency references.

Figure 8 shows the experimentally measured pulse after the medium and the theoretical prediction. We can see that the theoretical prediction matches the experimental data within the precision of the experiment; no fit parameters are used. The pulse shows a large time delay which is accurately predicted by the theory. This gives evidence that the refractive index spectrum predicted by ElecSus is accurate.

6. Conclusions and outlook

We have presented a computer program to calculate the electric susceptibility of an alkali-metal vapour, and we describe the underlying model used. The program can be used to design optical devices such as Faraday filters, and laser frequency stabilising references. The fitting routines provided in the program allow the user to measure experimental parameters (such as temperature or magnetic field).

We have modelled the D-lines of Na, K, Rb and Cs; a future version will include Li. Also, extending the program beyond D-line transitions may prove useful. For example, extending the model to include transitions between excited states may allow
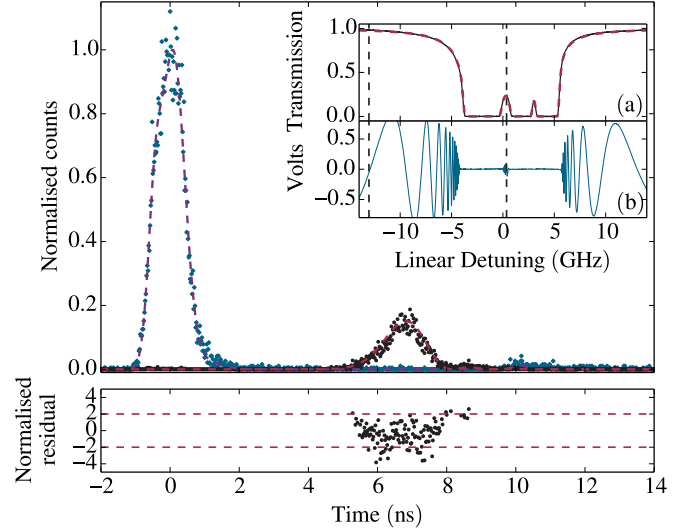

Figure 8: (Colour online) Slowlight pulse propagation through a 2 mm long rubidium vapour at natural abundance. The (black) dots and (blue) diamonds show the number of photons counted as a function of time (20 ps bin width) for a laser pulse with a carrier detuning near and far from resonance respectively. The counting was completed after approximately 100 k repetitions. The (purple) dashed line shows a multiple-Gaussian fit used to characterise the reference pulse. The (red) dashed line shows the theoretical prediction of pulse intensity measured after the cell. The data is normalised to the peak intensity of the reference pulse, while the time axis is centred at this peak. Underneath the graph is plotted the normalised residuals, which show good agreement (bins with less than 5 counts were omitted since they have been judged statistically insignificant [63]). Inset (a) shows a theoretical fit to a CW experimental transmission scan, performed immediately after the pulse experiment in order to extract the number density temperature and Doppler temperature of the medium. These taken to be 179.4 °C and 189.6 °C respectively. Inset (b) shows a Faraday signal from a 75 mm long cell used to stabilise the frequency of the laser [9] during the experiment. The black vertical dashed lines show the locking points used to stabilise the carrier detuning to (354 ± 2) MHz, and to (-13.0 ± 0.1) GHz when measuring the reference pulse.

modelling of excited state Faraday anomalous dispersion filters (ESFADOF) [70–72].

Working with atoms in confined geometries such as nanometric thin cells [73] or hollow-core fibres [74–79], introduces deviations of the atomic lineshape from the simple Voigt profile. This is due to effects such as atom-surface interactions [80–82] and Dicke narrowing. Extending the model to allow different atomic lineshapes has already been shown to accurately account for these effects [1, 82], and so we intend to extend ElecSus to include these effects.

Figure 8 motivates future versions of the program to contain a pulse propagation feature. It again shows that the medium can be accurately probed at GHz bandwidth [83]. As such fitting to a nanosecond pulse should allow further improvements to accuracy and facilitate observation of dynamics on short timescales [84].

9

Appendix A. Vapour pressure equations and isotopic abundances

Here we list the vapour pressure equations that are used to find the atomic number density as a function of temperature, T. The equations for all four elements are of the form

$$\log_{10}(p[\text{atm}]) = A + B(T[\text{K}])^{-1} + C\log_{10}(T[\text{K}]), \tag{A.1}$$

where p is the vapour pressure, values in square brackets denote the units of the corresponding variables and A, B and C are constants specific to the element and its phase (solid or liquid). Table A.1 shows the values of the constants used for the ElecSus program. All the constants were taken from the "precise" values given in [69]. The atomic number density can then be found from

Element (phase)	A	B	C
Na (solid)	5.298	−5603	
Na (liquid)	8.400	−5634	−1.1748
K (solid)	4.961	−4646	
K (liquid)	8.233	−4693	−1.2403
Rb (solid)	4.857	−4215	
Rb (liquid)	8.316	−4275	−1.3102
Cs (solid)	4.711	−3999	
Cs (liquid)	8.232	−4062	−1.3359

Table A.1: Values of the constants used in eq A.1 to determine the vapour pressure. Values are taken from [69].

the pressure by assuming an ideal gas,

$$\mathcal{N} = \frac{p}{k_\text{B}T} \tag{A.2}$$

The conversion factor for atmospheres to pascals (1 atm = 101325 Pa) is also used in order to get the number density in units of atoms/m^3. It should be noted these equations will give the elemental atomic number density and so they need to be reduced by the appropriate factor when considering one isotope of the element. For example the number density of ^{87}Rb in a naturally abundant vapour will be given by the Rb elemental number density multiplied by 0.2783. Table A.2 shows the natural isotopic abundances.

Element	Mass number	Abundance (%)
Na	23	100
K	39	93.2581
	40	0.0117
	41	6.7302
Rb	85	72.17
	87	27.83
Cs	133	100

Table A.2: Natural abundances of sodium, potassium, rubidium and caesium. Taken from [85].

Appendix B. Physical constants

This section lists the values of the physical constants used by ElecSus.

Quantity	Symbol	Value
Electron spin g-factor	g_S	2.00231930436153(53)
Bohr magneton	μ_B	$9.27400968(20) \times 10^{-24}$ J·T^{-1}
Boltzmann constant	k_B	$1.3806488(13) \times 10^{-23}$ J·K^{-1}
Atomic mass unit	u	$1.660538921(73) \times 10^{-27}$ kg
Vacuum permittivity	ϵ_0	$8.854187817620389 \times 10^{-12}$ F·m^{-1}
Bohr radius	a_0	$5.2917721092(17) \times 10^{-11}$ m
Reduced Planck constant	$\hbar$	$1.054571726(47) \times 10^{-34}$ J·s
Speed of light	c	299792458 m·s^{-1}
Elementary charge	e	$1.602176565(35) \times 10^{-19}$ C

Table B.3: Fundamental constants which are loaded from SciPy v0.13.2 library [86], which in turn come from the 2010 CODATA recommended values [87]. Updating SciPy may automatically update these physical constants for ElecSus.

Element	Quantity	Symbol	Value	Reference
	Linecentre wavelength	λ_0	589.7558147 nm	defined
Na	Linecentre frequency	ν_0	508.3331958 THz	defined
	Natural linewidth (FWHM)	Γ_0	$2\pi \times 9.765(13)$ MHz	[88]
	Linecentre wavelength	λ_0	770.108353667 nm	defined
K	Linecentre frequency	ν_0	389.286074580 THz	defined
	Natural linewidth (FWHM)	Γ_0	$2\pi \times 5.956(11)$ MHz	[89]
	Linecentre wavelength	λ_0	794.978969380 nm	defined
Rb	Linecentre frequency	ν_0	377.107407299 THz	defined
	Natural linewidth (FWHM)	Γ_0	$2\pi \times 5.746(8)$ MHz	[90]
	Linecentre wavelength	λ_0	894.59295986 nm	defined
Cs	Linecentre frequency	ν_0	335.116048807 THz	defined
	Natural linewidth (FWHM)	Γ_0	$2\pi \times 4.584(8)$ MHz	[91]

Table B.4: Constants related to the D$_1$ line. The linecentre refers to the definition of zero global detuning.

Element	Quantity	Symbol	Value	Reference
	Linecentre wavelength	λ_0	589.1583264 nm	defined
Na	Linecentre frequency	ν_0	508.8487162 THz	defined
	Natural linewidth (FWHM)	Γ_0	$2\pi \times 9.792(13)$ MHz	[88]
	Linecentre wavelength	λ_0	766.700890602 nm	defined
K	Linecentre frequency	ν_0	391.01618594 THz	defined
	Natural linewidth (FWHM)	Γ_0	$2\pi \times 6.035(11)$ MHz	[89]
	Linecentre wavelength	λ_0	780.2413272 nm	defined
Rb	Linecentre frequency	ν_0	384.2304266 THz	defined
	Natural linewidth (FWHM)	Γ_0	$2\pi \times 6.065(9)$ MHz	[90]
	Linecentre wavelength	λ_0	852.34727582 nm	defined
Cs	Linecentre frequency	ν_0	351.72571850 THz	defined
	Natural linewidth (FWHM)	Γ_0	$2\pi \times 5.225(7)$ MHz	[92]

Table B.5: Constants related to the D$_2$ line. The linecentre refers to the definition of zero global detuning.

Quantity	Symbol	Value	Reference
Nuclear spin	I	5/2	
Nuclear spin g-factor	g_I'	−0.00029364	[93]
Magnetic dipole constant for $5^2S_{1/2}$	A_{hf}	1011.910813 MHz·h	[93]
Magnetic dipole constant for $5^2P_{1/2}$	A_{hf}	120.640 MHz·h	[94]
Magnetic dipole constant for $5^2P_{3/2}$	A_{hf}	25.038 MHz·h	[95]
Electric quadrupole constant for $5^2P_{3/2}$	B_{hf}	26.011 MHz·h	[95]
Isotope shift (D$_1$)	E_{iso}	−21.624 MHz·h	[94]
Isotope shift (D$_2$)	E_{iso}	−21.734 MHz·h	[96]
Mass	m	84.911789732 u	[97]

Table B.6: Constants related to the [85]Rb atom. Isotope shifts are relative to the weighted linecentre of a naturally abundant rubidium vapour.

Quantity	Symbol	Value	Reference
Nuclear spin	I	3/2	
Nuclear spin g-factor	g_I'	-0.0009951414	[93]
Magnetic dipole constant for $5^2S_{1/2}$	A_{hf}	3417.341305452145 MHz·h	[98]
Magnetic dipole constant for $5^2P_{1/2}$	A_{hf}	406.147 MHz·h	[94]
Magnetic dipole constant for $5^2P_{3/2}$	A_{hf}	84.7185 MHz·h	[99]
Electric quadrupole constant for $5^2P_{3/2}$	B_{hf}	12.4965 MHz·h	[99]
Mass	m	86.909180520 u	[97]
Isotope shift (D$_1$)	E_{iso}	56.077 MHz·h	[94]
Isotope shift (D$_2$)	E_{iso}	56.361 MHz·h	[96]

Table B.7: Constants related to the [87]Rb atom. Isotope shifts are relative to the weighted linecentre of a naturally abundant rubidium vapour.

References

[1] J. Keaveney, A. Sargsyan, U. Krohn, I. G. Hughes, D. Sarkisyan, C. S. Adams, Phys. Rev. Lett. 108 (2012) 173601. URL: http://link.aps.org/doi/10.1103/PhysRevLett.108.173601. doi:10.1103/PhysRevLett.108.173601.

[2] A. Sargsyan, G. Hakhumyan, C. Leroy, Y. Pashayan-Leroy, A. Papoyan, D. Sarkisyan, Opt. Lett. 37 (2012) 1379–81. URL: http://www.ncbi.nlm.nih.gov/pubmed/22513692.

[3] B. Julsgaard, A. Kozhekin, E. S. Polzik, Nature 413 (2001) 400. URL: http://www.ncbi.nlm.nih.gov/pubmed/11574882. doi:10.1038/35096524.

[4] U. Vogl, M. Weitz, Nature 461 (2009) 70–3. URL: http://www.ncbi.nlm.nih.gov/pubmed/19727195. doi:10.1038/nature08203.

[5] C. Carr, R. Ritter, C. G. Wade, C. S. Adams, K. J. Weatherill, Phys. Rev. Lett. 111 (2013) 113901. URL: http://link.aps.org/doi/10.1103/PhysRevLett.111.113901. doi:10.1103/PhysRevLett.111.113901.

[6] P. D. D. Schwindt, S. Knappe, V. Shah, L. Hollberg, J. Kitching, L.-A. Liew, J. Moreland, Appl. Phys. Lett. 85 (2004) 6409. URL: http://link.aip.org/link/APPLAB/v85/i26/p6409/s1&Agg=doi. doi:10.1063/1.1839274.

[7] S. Knappe, V. Shah, P. D. D. Schwindt, L. Hollberg, J. Kitching, L.-A. Liew, J. Moreland, Appl. Phys. Lett. 85 (2004) 1460. URL: http://link.aip.org/link/APPLAB/v85/i9/p1460/s1&Agg=doi. doi:10.1063/1.1787942.

[8] C. Affolderbach, G. Mileti, Rev. Sci. Instrum. 76 (2005) 073108. URL: http://link.aip.org/link/RSINAK/v76/i7/p073108/s1&Agg=doi. doi:10.1063/1.1979493.

[9] A. L. Marchant, S. Händel, T. P. Wiles, S. A. Hopkins, C. S. Adams, S. L. Cornish, Opt. Lett. 36 (2011) 64. URL: http://www.ncbi.nlm.nih.gov/pubmed/21209688.

[10] M. A. Zentile, R. Andrews, L. Weller, S. Knappe, C. S. Adams, I. G. Hughes, J. Phys. B At. Mol. Opt. Phys. 47 (2014) 075005. URL: http://stacks.iop.org/0953-4075/47/i=7/a=075005?key=crossref.531fd3098eb98a338bf213c3bfd5ada3. doi:10.1088/0953-4075/47/7/075005. arXiv:1401.1659.

[11] A. Vernier, S. Franke-Arnold, E. Riis, A. S. Arnold, Opt. Express 18 (2010) 17020–6. URL: http://www.ncbi.nlm.nih.gov/pubmed/20721090.

[12] G. Walker, A. S. Arnold, S. Franke-Arnold, Phys. Rev. Lett. 108 (2012) 243601. URL: http://link.aps.org/doi/10.1103/PhysRevLett.108.243601. doi:10.1103/PhysRevLett.108.243601.

[13] B. Julsgaard, J. Sherson, J. I. Cirac, J. Fiurásek, E. S. Polzik, Nature 432 (2004) 482–6. URL: http://www.ncbi.nlm.nih.gov/pubmed/15565148. doi:10.1038/nature03064.

[14] D. G. England, P. S. Michelberger, T. F. M. Champion, K. F. Reim, K. C. Lee, M. R. Sprague, X.-M. Jin, N. K. Langford, W. S. Kolthammer, J. Nunn, I. A. Walmsley, J. Phys. B At. Mol. Opt. Phys. 45 (2012) 124008. URL: http://stacks.iop.org/0953-4075/45/i=12/a=124008?key=crossref.fd7a366917fde377df6cdceca0f6ea7b.

[15] P. Siddons, C. S. Adams, C. Ge, I. G. Hughes, J. Phys. B At. Mol. Opt. Phys. 41 (2008) 155004. URL: http://dx.doi.org/10.1088/0953-4075/41/15/155004. doi:10.1088/0953-4075/41/15/155004.

[16] J. Menders, K. Benson, S. H. Bloom, C. S. Liu, E. Korevaar, Opt. Lett. 16 (1991) 846–8. URL: http://www.ncbi.nlm.nih.gov/pubmed/19776805.

[17] H. Chen, C. Y. She, P. Searcy, E. Korevaar, Optics Letters 18 (1993) 1019. URL: http://www.opticsinfobase.org/abstract.cfm?URI=ol-18-12-1019. doi:10.1364/OL.18.001019.

[18] R. P. Abel, U. Krohn, P. Siddons, I. G. Hughes, C. S. Adams, Opt. Lett. 34 (2009) 3071. URL: http://dx.doi.org/10.1364/OL.34.003071. doi:10.1364/OL.34.003071.

[19] J. A. ZieliÅska, F. A. Beduini, N. Godbout, M. W. Mitchell, Opt. Lett. 37 (2012) 524–6. URL: http://dx.doi.org/10.1364/OL.37.000524. doi:10.1364/OL.37.000524.

[20] L. Weller, K. S. Kleinbach, M. A. Zentile, S. Knappe, I. G. Hughes, C. S. Adams, Opt. Lett. 37 (2012) 3405. doi:10.1364/OL.37.003405.

[21] D. Budker, M. Romalis, Nat. Phys. 3 (2007) 227–234. URL: http://www.nature.com/doifinder/10.1038/nphys566. doi:10.1038/nphys566.

[22] G. Casa, A. Castrillo, G. Galzerano, R. Wehr, A. Merlone, D. Di Serafino, P. Laporta, L. Gianfrani, Phys. Rev. Lett. 100 (2008) 200801. URL: http://link.aps.org/doi/10.1103/PhysRevLett.100.200801. doi:10.1103/PhysRevLett.100.200801.

[23] M. Triki, C. Lemarchand, B. Darquié, P. L. T. Sow, V. Roncin, C. Chardonnet, C. Daussy, Phys. Rev. A 85 (2012) 062510. doi:10.1103/PhysRevA.85.062510.

[24] G.-W. Truong, J. Anstie, E. May, T. Stace, A. N. Luiten, Phys. Rev. A 86 (2012) 030501. URL: http://link.aps.org/doi/10.1103/PhysRevA.86.030501. doi:10.1103/PhysRevA.86.030501.

[25] Z. Wu, M. Kitano, W. Happer, M. Hou, J. Daniels, Appl. Opt. 25 (1986) 4483. URL: http://www.opticsinfobase.org/abstract.cfm?URI=ao-25-23-4483. doi:10.1364/AO.25.004483.

[26] E. Vliegen, S. Kadlecek, L. W. Anderson, T. G. Walker, C. J. Erickson, W. Happer, Nucl. Instruments Methods Phys. Res. Sect. A Accel. Spectrometers, Detect. Assoc. Equip. 460 (2001) 444–450. URL: http://linkinghub.elsevier.com/retrieve/pii/S0168900200010615. doi:10.1016/S0168-9002(00)01061-5.

[27] U. Rapol, A. Wasan, V. Natarajan, Phys. Rev. A 64 (2001) 023402. URL: http://link.aps.org/doi/10.1103/PhysRevA.64.023402. doi:10.1103/PhysRevA.64.023402.

[28] K. L. Moore, T. P. Purdy, K. W. Murch, S. Leslie, S. Gupta, D. M. Stamper-Kurn, Rev. Sci. Instrum. 76 (2005) 023106. URL: http://scitation.aip.org/content/aip/journal/rsi/76/2/10.1063/1.1841852. doi:10.1063/1.1841852.

[29] D. R. Scherer, D. B. Fenner, J. M. Hensley, J. Vac. Sci. Technol. A 30 (2012) 061602. doi:http://dx.doi.org/10.1116/1.4757950.

[30] J. Su, D.-z. Guo, in: 2009 IEEE Int. Freq. Control Symp. Jt. with 22nd Eur. Freq. Time forum, IEEE, 2009, pp. 1016–1018. URL: http://ieeexplore.ieee.org/lpdocs/epic03/wrapper.htm?arnumber=5168346. doi:10.1109/FREQ.2009.5168346.

[31] T. Baluktsian, C. Urban, T. Bublat, H. Giessen, R. Löw, T. Pfau, Opt. Lett. 35 (2010) 1950–2. URL: http://www.ncbi.nlm.nih.gov/pubmed/20548349.

[32] P. Knapkiewicz, J. Dziuban, R. Walczak, L. Mauri, P. Dziuban, C. Gorecki, Procedia Eng. 5 (2010) 721–724. URL: http://linkinghub.elsevier.com/retrieve/pii/S1877705810007575. doi:10.1016/j.proeng.2010.09.210.

[33] K. Tsujimoto, K. Ban, Y. Hirai, K. Sugano, T. Tsuchiya, N. Mizutani, O. Tabata, J. Micromechanics Microengineering 23 (2013) 115003. URL: http://stacks.iop.org/0960-1317/23/i=11/a=115003?key=crossref.bd22504df11af1d2ac2e060aa2017784. doi:10.1088/0960-1317/23/11/115003.

[34] L. Weller, R. J. Bettles, P. Siddons, C. S. Adams, I. G. Hughes, J. Phys. B At. Mol. Opt. Phys. 44 (2011) 195006. URL: http://stacks.iop.org/0953-4075/44/i=19/a=195006?key=crossref.6053c04e063ad80a26ce7648067c84ae. doi:10.1088/0953-4075/44/19/195006.

[35] L. Weller, T. Dalton, P. Siddons, C. S. Adams, I. G. Hughes, J. Phys. B At. Mol. Opt. Phys. 45 (2012) 055001. URL: http://stacks.iop.org/0953-4075/45/i=5/a=055001?key=crossref.ac90c91eb2c2d263602908d6ff929f29. doi:10.1088/0953-4075/45/5/055001.

[36] B. H. Bransden, C. J. Joachain, Physics of Atoms and Molecules, 2nd ed., Pearson Education Limited, Harlow, 2003.

[37] L. Weller, R. J. Bettles, C. L. Vaillant, M. A. Zentile, R. M. Potvliege, C. S. Adams, I. G. Hughes (2013) 1–8. URL: http://arxiv.org/abs/1308.0129. arXiv:1308.0129.

[38] L. Weller, K. S. Kleinbach, M. A. Zentile, S. Knappe, C. S. Adams, I. G. Hughes, J. Phys. B At. Mol. Opt. Phys. 45 (2012) 215005. URL: http://stacks.iop.org/0953-4075/45/i=21/a=215005?key=crossref.c040f761efe2795ec00dca983ff20910. doi:10.1088/0953-4075/45/21/215005.

[39] J. D. Jackson, Classical Electrodynamics, third ed., Wiley, 1999.

[40] L. V. Hau, S. Harris, Z. Dutton, C. H. Behroozi, Nature 397 (1999) 594–598. URL: http://www.nature.com/nature/journal/v397/n6720/abs/397594a0.html.

[41] L. J. Wang, A. Kuzmich, A. Dogariu, Nature 406 (2000) 277–9. URL: http://www.ncbi.nlm.nih.gov/pubmed/10917523. doi:10.1038/

35018520.

[42] J. Keaveney, I. G. Hughes, A. Sargsyan, D. Sarkisyan, C. S. Adams, Phys. Rev. Lett. 109 (2012) 233001. URL: http://link.aps.org/doi/10.1103/PhysRevLett.109.233001. doi:10.1103/PhysRevLett.109.233001.

[43] L. Brillouin, Wave Propagation and Group Velocity, first ed., Academic Press, 1960.

[44] A. Corney, Atomic and Laser Spectroscopy, Oxford University Press, Oxford, 1977.

[45] S. J. Blundell, K. M. Blundell, Concepts in Thermal Physics, Oxford University Press, 2009. URL: http://www.oxfordscholarship.com/view/10.1093/acprof:oso/9780199562091.001.0001/acprof-9780199562091. doi:10.1093/acprof:oso/9780199562091.001.0001.

[46] C. J. Foot, Atomic Physics, first ed., Oxford University Press, 2005.

[47] D. A. Smith, I. G. Hughes, Am. J. Phys. 72 (2004) 631. URL: http://link.aip.org/link/AJPIAS/v72/i5/p631/s1&Agg=doi. doi:10.1119/1.1652039.

[48] B. E. Sherlock, I. G. Hughes, Am. J. Phys. 77 (2009) 111. URL: http://link.aip.org/link/AJPIAS/v77/i2/p111/s1&Agg=doi. doi:10.1119/1.3013197.

[49] S. Ro Shin, H.-R. Noh, J. Phys. Soc. Japan 78 (2009) 084302. URL: http://journals.jps.jp/doi/abs/10.1143/JPSJ.78.084302. doi:10.1143/JPSJ.78.084302.

[50] T. M. Stace, G.-W. Truong, J. Anstie, E. F. May, A. N. Luiten, Phys. Rev. A 86 (2012) 012506. URL: http://link.aps.org/doi/10.1103/PhysRevA.86.012506. doi:10.1103/PhysRevA.86.012506.

[51] R. Dicke, Physical Review 89 (1953) 472–473. URL: http://link.aps.org/doi/10.1103/PhysRev.89.472. doi:10.1103/PhysRev.89.472.

[52] P. Siddons, C. S. Adams, I. G. Hughes, J. Phys. B At. Mol. Opt. Phys. 42 (2009) 175004. URL: http://stacks.iop.org/0953-4075/42/i=17/a=175004?key=crossref.31a57cd8a13d53e52ac8d09004992fdb. doi:10.1088/0953-4075/42/17/175004.

[53] P. Siddons, J. Phys. B At. Mol. Opt. Phys. 47 (2014) 093001. URL: http://stacks.iop.org/0953-4075/47/i=9/a=093001?key=crossref.1270f2d4349154e2d4a29a54d671ed23. doi:10.1088/0953-4075/47/9/093001.

[54] V. Gerginov, A. Derevianko, C. Tanner, Phys. Rev. Lett. 91 (2003) 072501. URL: http://link.aps.org/doi/10.1103/PhysRevLett.91.072501. doi:10.1103/PhysRevLett.91.072501.

[55] A. R. Edmonds, Angular momentum in quantum mechanics, 2nd, fourt ed., Princeton University Press, Princeton, New Jersey, 1996.

[56] B. Schaefer, E. Collett, R. Smyth, D. Barrett, B. Fraher, Am. J. Phys. 75 (2007) 163. URL: http://link.aip.org/link/AJPIAS/v75/i2/p163/s1&Agg=doi. doi:10.1119/1.2386162.

[57] W. Yuan, W. Shen, Y. Zhang, X. Liu, Optics Express 22 (2014) 11011. URL: http://www.opticsinfobase.org/abstract.cfm?URI=oe-22-9-11011. doi:10.1364/OE.22.011011.

[58] A. Millett-Sikking, I. G. Hughes, P. Tierney, S. L. Cornish, J. Phys. B At. Mol. Opt. Phys. 40 (2007) 187–198. URL: http://stacks.iop.org/0953-4075/40/i=1/a=017?key=crossref.f0bbbf1fd11b645adf0ace1efef951ee. doi:10.1088/0953-4075/40/1/017.

[59] C. Lee, G. Z. Iwata, E. Corsini, J. M. Higbie, S. Knappe, M. P. Ledbetter, D. Budker, The Review of scientific instruments 82 (2011) 043107. URL: http://www.ncbi.nlm.nih.gov/pubmed/21528995. doi:10.1063/1.3568824.

[60] R. Clark Jones, Journal of the Optical Society of America 31 (1941) 488. URL: http://www.opticsinfobase.org/abstract.cfm?URI=josa-31-7-488. doi:10.1364/JOSA.31.000488.

[61] E. Hecht, Optics, fourth ed., Addison Wesley, 2002.

[62] J. D. Hunter, Computing In Science & Engineering 9 (2007) 90–95. doi:10.1109/MCSE.2007.55.

[63] I. G. Hughes, T. P. A. Hase, Measurements and their Uncertainties: A Practical Guide to Modern Error Analysis, first ed., Oxford University Press, 2010.

[64] S. G. Johnson, Faddeeva function implementation, 2014. URL: http://ab-initio.mit.edu/Faddeeva.

[65] S. Russel, P. Norvig, Artificial Intelligence: A Modern Approach, second

[66] S. Kirkpatrick, C. D. Gelatt, M. P. Vecchi, Science (80-.). 220 (1983) 671–680.

[67] N. Metropolis, A. W. Rosenbluth, M. N. Rosenbluth, A. H. Teller, E. Teller, J. Chem. Phys. 21 (1953) 1087. URL: http://link.aip.org/link/JCPSA6/v21/i6/p1087/s1&Agg=doi. doi:10.1063/1.1699114.

[68] M. Lundy, A. Mees, Math. Program. 34 (1986) 111. URL: http://www.springerlink.com/index/R00N02366342UV61.pdf.

[69] C. B. Alcock, V. P. Itkin, M. K. Horrigan, Can. Metall. Q. 23 (1984) 309–313. URL: http://dx.doi.org/10.1179/000844384795483058. doi:10.1179/000844384795483058.

[70] R. I. Billmers, S. K. Gayen, M. F. Squicciarini, V. M. Contarino, W. J. Scharpf, D. M. Allocca, Opt. Lett. 20 (1995) 106–8. URL: http://www.ncbi.nlm.nih.gov/pubmed/19855811.

[71] L. Zhang, J. Tang, Opt. Commun. 152 (1998) 275–279. URL: http://linkinghub.elsevier.com/retrieve/pii/S0030401898001990. doi:10.1016/S0030-4018(98)00199-0.

[72] A. Rudolf, T. Walther, Opt. Lett. 37 (2012) 4477. URL: http://www.opticsinfobase.org/abstract.cfm?URI=ol-37-21-4477. doi:10.1364/OL.37.004477.

[73] D. Sarkisyan, D. Bloch, A. Papoyan, M. Ducloy, Opt. Commun. 200 (2001) 201–208. URL: http://linkinghub.elsevier.com/retrieve/pii/S0030401801016042. doi:10.1016/S0030-4018(01)01604-2.

[74] M. Bajcsy, S. Hofferberth, V. Balic, T. Peyronel, M. Hafezi, A. Zibrov, V. Vuletic, M. Lukin, Phys. Rev. Lett. 102 (2009) 203902. URL: http://link.aps.org/doi/10.1103/PhysRevLett.102.203902. doi:10.1103/PhysRevLett.102.203902.

[75] V. Venkataraman, K. Saha, A. L. Gaeta, Nat. Photonics 7 (2012) 138–141. URL: http://dx.doi.org/10.1038/nphoton.2012.283. doi:10.1038/nphoton.2012.283.

[76] C. Perrella, P. S. Light, J. D. Anstie, F. Benabid, T. M. Stace, a. G. White, a. N. Luiten, Phys. Rev. A 88 (2013) 013819. URL: http://link.aps.org/doi/10.1103/PhysRevA.88.013819. doi:10.1103/PhysRevA.88.013819.

[77] G. Epple, K. S. Kleinbach, T. G. Euser, N. Y. Joly, T. Pfau, P. S. J. Russell, R. Löw, Nature communications 5 (2014) 4132. URL: http://www.ncbi.nlm.nih.gov/pubmed/24942281. doi:10.1038/ncomms5132.

[78] M. R. Sprague, P. S. Michelberger, T. F. M. Champion, D. G. England, J. Nunn, X.-M. Jin, W. S. Kolthammer, A. Abdolvand, P. S. J. Russell, I. A. Walmsley, Nat. Photonics 8 (2014) 287–291. URL: http://www.nature.com/doifinder/10.1038/nphoton.2014.45. doi:10.1038/nphoton.2014.45.

[79] F. Haas, J. Volz, R. Gehr, J. Reichel, J. Estève, Science 180 (2014). URL: http://www.ncbi.nlm.nih.gov/pubmed/24674870. doi:10.1126/science.1248905.

[80] H. B. G. Casimir, D. Polder, Phys. Rev. 73 (1948) 360–372. URL: http://dx.doi.org/10.1103/PhysRev.73.360. doi:10.1103/PhysRev.73.360.

[81] H. Bender, C. Stehle, C. Zimmermann, S. Slama, J. Fiedler, S. Scheel, S. Y. Buhmann, V. N. Marachevsky, Phys. Rev. X 4 (2014) 011029. URL: http://link.aps.org/doi/10.1103/PhysRevX.4.011029. doi:10.1103/PhysRevX.4.011029.

[82] K. A. Whittaker, J. Keaveney, I. G. Hughes, A. Sargsyan, D. Sarkisyan, C. S. Adams, Physical Review Letters 112 (2014) 253201. URL: http://link.aps.org/doi/10.1103/PhysRevLett.112.253201. doi:10.1103/PhysRevLett.112.253201.

[83] P. Siddons, N. C. Bell, Y. Cai, C. S. Adams, I. G. Hughes, Nat. Photonics 3 (2009) 225–229. URL: http://www.nature.com/nphoton/journal/v3/n4/abs/nphoton.2009.27.html. doi:10.1038/NPHOTON.2009.27.

[84] R. Löw, T. Pfau, Nat. Photonics 3 (2009) 197–199. URL: http://www.nature.com/doifinder/10.1038/nphoton.2009.41. doi:10.1038/nphoton.2009.41.

[85] K. J. R. Rosman, P. D. P. Taylor, Pure Appl. Chem. 70 (1998) 217–235. URL: http://iupac.org/publications/pac/70/1/0217/. doi:10.1351/pac199870010217.

[86] E. Jones, T. Oliphant, P. Peterson, et al., SciPy: Open source scientific tools for Python, 2001–. URL: http://www.scipy.org/.

[87] P. J. Mohr, B. N. Taylor, D. B. Newell, Rev. Mod. Phys.

84 (2012) 1527–1605. URL: `http://link.aps.org/doi/10.1103/RevModPhys.84.1527`. doi:10.1103/RevModPhys.84.1527.

[88] U. Volz, M. Majerus, H. Liebel, A. Schmitt, H. Schmoranzer, Physical Review Letters 76 (1996) 2862–2865. URL: `http://link.aps.org/doi/10.1103/PhysRevLett.76.2862`. doi:10.1103/PhysRevLett.76.2862.

[89] H. Wang, P. L. Gould, W. C. Stwalley, The Journal of Chemical Physics 106 (1997) 7899. URL: `http://scitation.aip.org/content/aip/journal/jcp/106/19/10.1063/1.473804`. doi:10.1063/1.473804.

[90] U. Volz, H. Schmoranzer, Phys. Scr. T65 (1996) 48–56. URL: `http://stacks.iop.org/1402-4896/1996/i=T65/a=007?key=crossref.308955f823ef0fbebc7e5e7dab6b1e0c`. doi:10.1088/0031-8949/1996/T65/007.

[91] J. Amini, H. Gould, Physical Review Letters 91 (2003) 153001. URL: `http://link.aps.org/doi/10.1103/PhysRevLett.91.153001`. doi:10.1103/PhysRevLett.91.153001.

[92] J. F. Sell, B. M. Patterson, T. Ehrenreich, G. Brooke, J. Scoville, R. J. Knize, Physical Review A 84 (2011) 010501. URL: `http://link.aps.org/doi/10.1103/PhysRevA.84.010501`. doi:10.1103/PhysRevA.84.010501.

[93] E. Arimondo, M. Inguscio, P. Violino, Rev. Mod. Phys. 49 (1977) 31–75. URL: `http://link.aps.org/doi/10.1103/RevModPhys.49.31`. doi:10.1103/RevModPhys.49.31.

[94] A. Banerjee, D. Das, V. Natarajan, Europhys. Lett. 65 (2004) 172. URL: `http://stacks.iop.org/0295-5075/65/i=2/a=172?key=crossref.3f31cde52c3d64256aa82cdddcaef69a`. doi:10.1209/epl/i2003-10069-3.

[95] U. Rapol, A. Krishna, V. Natarajan, Eur. Phys. J. D - At. Mol. Opt. Phys. 23 (2003) 185–188. URL: `http://www.springerlink.com/Index/10.1140/epjd/e2003-00069-9`. doi:10.1140/epjd/e2003-00069-9.

[96] G. P. Barwood, P. Gill, W. R. C. Rowley, Appl. Phys. B Photophysics Laser Chem. 53 (1991) 142–147. URL: `http://link.springer.com/10.1007/BF00330229`. doi:10.1007/BF00330229.

[97] M. Bradley, J. Porto, S. Rainville, J. Thompson, D. Pritchard, Phys. Rev. Lett. 83 (1999) 4510–4513. URL: `http://link.aps.org/doi/10.1103/PhysRevLett.83.4510`. doi:10.1103/PhysRevLett.83.4510.

[98] S. Bize, Y. Sortais, M. S. Santos, C. Mandache, A. Clairon, C. Salomon, Europhys. Lett. 45 (1999) 558–564. URL: `http://stacks.iop.org/0295-5075/45/i=5/a=558?key=crossref.666131c213ed5b0ba506c88d36908ac8`. doi:10.1209/epl/i1999-00203-9.

[99] J. Ye, S. Swartz, P. Jungner, J. L. Hall, Opt. Lett. 21 (1996) 1280. URL: `http://www.ncbi.nlm.nih.gov/pubmed/19876325http://www.opticsinfobase.org/abstract.cfm?URI=ol-21-16-1280`. doi:10.1364/OL.21.001280.